Research Article

Cross-docking and molecular dynamic studies to achieve the potent antiviral HIV-1 nonnucleoside reverse transcriptase inhibitors

Suwicha Patnin[1], Arthit Makarasen[1*], Pongsit Vijitphan[1], Apisara Baicharoen[1], Wandee Sirithana[2] and Supanna Techasakul[1*]

Received: 17 August 2023
Revised: 2 October 2023
Accepted: 12 October 2023

ABSTRACT

Our objective in the present study is to describe and validate the procedures utilized to investigate a quinoline-based compound's potential as an anti-HIV-1 reverse transcriptase (HIV-1 RT) agent. Through the fusion of the pharmacophores found in the structural makeup of HIV-1 RT drugs, the quinoline derivatives 4-(2′,6′-dimethyl-4′-cyanophenoxy)-6-(4′′-cyanophenyl)-aminoquinoline **(1)** and 4-(2′,6′-dimethyl-4′-cyanophenoxy)-2-(4′′-cyanophenyl)-aminoquinoline **(2)** have been reported and developed. Using cross-docking, molecular docking, and molecular dynamic approaches, the binding interactions of nonnucleoside reverse transcriptase inhibitors (NNRTIs), quinoline derivatives, and HIV-1 RT were examined. When compared to the other conformations of HIV-1 RT, the cross-docking revealed that the 4G1Q.pdb conformation had the lowest binding energy values. According to the molecular docking evidence, **(2)** interacted with LYS101 residues by hydrogen bonding and with TYR181 and TRP229 residues via π-π stacking in the binding pocket of HIV-1 RT, similar to that of rilpivirine. Furthermore, molecular dynamics simulations showed that the binding affinity of **(1)** and **(2)** with HIV-1 RT was quite stable. The stronger binding of HIV-1 RT-**(2)** in comparison to HIV-1 RT-**(1)** was further corroborated by the binding free energy determined by MMPBSA and MMGBSA calculations.

Keywords: Cross-docking, Quinoline, Anti-HIV-1 activity, Molecular docking, Molecular Dynamic

[1] Department of Chemistry, Laboratory of Organic Synthesis, Chulabhorn Research Institute, Bangkok 10210, Thailand
[2] Faculty of Science and Technology, Suan Dusit University, Bangkok 10300, Thailand
*Corresponding authors, email: arthit@cri.or.th; supanna@cri.or.th

Introduction

The cause of acquired immune deficiency syndrome (AIDS) has been identified as the human immunodeficiency virus type 1 (HIV-1). In infected cells, the HIV-1 reverse transcriptase (RT) enzyme catalyzes the reverse transcription of the viral RNA genome to double-stranded DNA [1,2]. Therefore, the identification of HIV-1 RT inhibitors is one of the key therapeutic plans for antiretroviral development. Nonnucleoside reverse transcriptase inhibitors (NNRTIs) are one of numerous HIV-1 RT inhibitors. Nonnucleoside reverse transcriptase inhibitors (NNRTIs) have currently been approved by the Federal Food and Drug Administration (FDA) for two generations [3,4]. The first-generation NNRTIs displayed broad anti-HIV-1 RT efficacy but were defenseless against common drug-resistance mutations such as efavirenz (EFV), delavirdine (DLV), and nevirapine (NVP) [5,6]. Second-generation drugs, such as etravirine (ETR), rilpivirine (RPV), and talviraline (HBY097), have shown considerable activity against drug-resistant strains of HIV-1 RT. However, the World Health Organization (WHO) has issued a warning about the developing trend of drug-resistant HIV, which is a threat to progress in the treatment and prevention of HIV infection [7-9]. As a result, ongoing research and development of anti-HIV-1 RT drugs have been reported.

In a recent study, we used a molecular hybridization technique to create amino-oxy-diarylquinolines by integrating NVP, EFV, ETR, and RPV pharmacophore templates. Following that, two groups of derivatives were synthesized: 2-amino-4-oxy-diarylquinolines and 4-amino-6-oxy-diarylquinolines. The inhibitory activity of these compounds against HIV-1 RT was evaluated using HIV-1 RT inhibition assays and molecular docking techniques. When compared to the 4-amino-6-oxy-diarylquinolines, the 2-amino-4-oxy-diarylquinolines demonstrated better binding affinity and more favorable binding interactions within the binding pocket of HIV-1 RT (PDB: 4G1Q) [10,11]. However, the protein database includes HIV-1 RT conformations such as 1FK9, 1KLM, 1VRT, 2IC3, 3MEC, and 4G1Q. The methodologies employed to examine the potential of a quinoline-based chemical as an anti-HIV-1 RT are discussed and described in this paper. 4-(2′,6′-dimethyl-4′-cyanophenoxy)-6-(4″-cyanophenyl)-aminoquinoline **(1)** and 4-(2′,6′-dimethyl-4′-cyanophenoxy)-6-(4″-cyanophenyl)-amino-quinoline **(2)** were chosen for this investigation due to their structural similarity to ETR and RPV, especially in terms of the side chain. Using cross-docking, molecular docking, and molecular dynamics simulations, we aim to validate the conformations of HIV-1 RT with NNRTIs and amino-oxy-diarylquinolines. Cross-docking approaches are used to dock several ligands and proteins utilizing different X-ray crystal structures of the same protein receptor to demonstrate a single protein receptor. Cross-docking is useful for anticipating the importance of the mechanism of drug-receptor binding interactions [12,13]. Molecular dynamics (MD) simulations were used to evaluate the binding stability of the ligands and the target protein, with the goal of investigating their stability and conformational changes in a solvent environment [14-16]. These findings provide critical information on binding location, binding energy, and ligand-receptor interactions, which is useful for drug design and complements prior and future research efforts.

Materials and Methods

Cross-docking between ligands with HIV-1 RT

The binding interactions of ligands with HIV-1 RT were simulated by molecular docking using AutoDock 4.2 (The Scripps Research Institute, La Jolla, CA, USA) [17]. The Lamarckian Genetic Algorithm (LGA) was selected with a population size of 150 individuals, and the number of genetic algorithm runs was set at 200. The grid box size was set at 80 x 80 x 80 Å, with a spacing of 0.375 Å. The docking results were explained by Accelrys Discovery Studio Client 4.0. Ligands were extracted from the crystal structures of HIV-1 RT, and hydrogen atoms were added. The geometries of the ligands, namely, efavirenz (EFV), delavirdine (DLV), nevirapine (NVP), talviraline (HBY097), etravirine (ETR), rilpivirine (RPV), 4-(2′,6′-dimethyl-4′-cyanophenoxy)-6-(4″-cyanophenyl)-aminoquinoline **(1)**, and 4-(2′,6′-dimethyl-4′-cyanophenoxy)-2-(4″-cyanophenyl)-aminoquinoline **(2)**, are shown in Figure 1. This was then fully optimized by density functional theory (DFT) at the B3LYP/6−31G(d,p) level implemented in Gaussian 09 [18]. The crystal structures of HIV-1 RT were obtained from the Protein Data Bank, such as 1FK9 [19], 1KLM [20], 1VRT [21], 2IC3 [22], 3MEC [23] and 4G1Q [24] (www.rcsb.org). The ligand and water in each protein structure were removed, and hydrogen atoms were added using Discovery Studio 2020 software (Accelrys, San Diego, CA, USA).

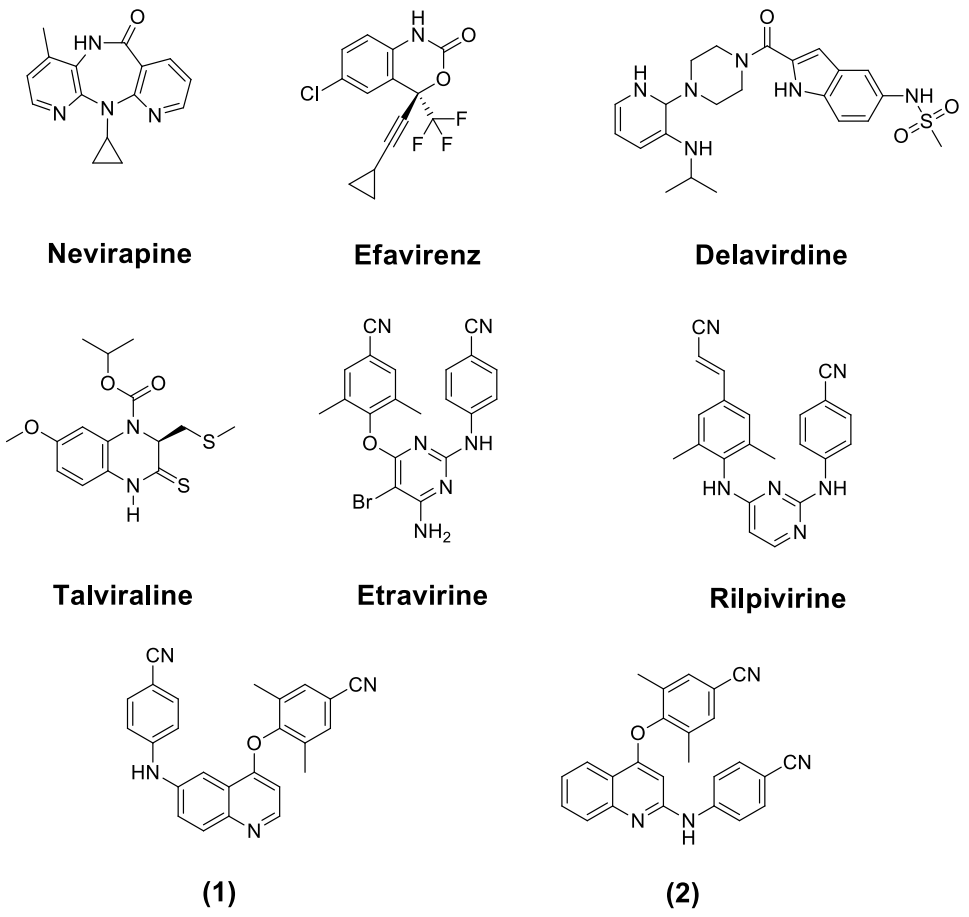

Figure 1 Structures of nonnucleoside reverse transcriptase inhibitors (NNRTIs) and quinoline derivatives.

Molecular Dynamic Simulations

The molecular dynamics (MD) simulations were conducted using the GROMACS (v2022.3) package (University of Groningen, Groningen, Netherlands). The AMBER99SB force field [25] was utilized in the MD simulations. MD simulations were performed to evaluate the stability and conformational changes of the complexes involving HIV-1 RT-RPV, HIV-1 RT-**(1)**, and HIV-1 RT-**(2)**. The complexes were solvated in a cubic box with the SPC216 water model. Energy minimization was carried out using the steepest descent method with 50,000 steps, followed by a 1000 ps equilibration of the entire system. The MD simulation was then run for 50 ns, maintaining a temperature of 310 K and a pressure of 1 bar. Additionally, the MD simulation results were visualized and analyzed using the Visual Molecular Dynamics (VMD) (University of Illinois Urbana-Champaign, Illinois, USA) [26].

Binding Free Energy Calculations

MMPBSA and MMGBSA are commonly used computational methods for studying protein-ligand interactions and drug design [27,28]. The binding free energies of HIV-1 RT-RPV, HIV-1 RT-**(1)**, and HIV-1 RT-**(2)** were calculated by collecting 500 snapshots from the last 50 ns of the MD simulation. The gmx_MMPBSA tool [29] was utilized to analyze these snapshots based on the Molecular Mechanics/Poisson-Boltzmann surface area (MMPBSA) approach. Additionally, the Molecular Mechanics/Generalized Born surface (MMGBSA) binding free energy calculation was performed in accordance with the MD simulation trajectories.

Results and Discussion

Cross-Docking between ligands with HIV-1 RT

The binding interaction of the ligands and HIV-1 RT was studied using molecular docking to understand the binding mode of the selected ligands with HIV-1 RT and provide information for drug design [30,31]. In this study, the X-ray crystal structures of the complex between the HIV-1 RT enzyme and its ligands, namely, 1FK9 (EFV), 1KLM (DLV), 1VRT (NVP), 2IC3 (HBY097), 3MEC (ETR), and 4G1Q (RPV), were used and docked to perform a cross-docking method to find a suitable crystal structure for HIV-1 RT inhibitor. The structures of the ligands are shown in Figure 1. The results showed that the binding energy values between the promising ligands and HIV-1 RT ranged from -6.69 to -12.62 kcal/mol, as shown in Table 1. RPV displayed the lowest binding energy value of -12.62 kcal/mol with 4G1Q, whereas HBY097 had the highest binding energy value of -6.69 kcal/mol with 2IC3, compared with other ligands and proteins, as shown in Table 1.

Table 1 The results of cross-docking between NNRTI drugs (NVP, EFV, DLV, HBY097, ETR, and RPV) with HIV-1 RT.

Ligand	Protein code of HIV-1 RT Binding energy (kcal/mol)					
	1VRT	1FK9	1KLM	2IC3	3MEC	4G1Q
NVP	-8.64	-8.27	-8.19	-6.96	7.67	-8.39
EFV	-9.94	-10.85	-9.10	-8.86	-8.82	-9.25
DLV	-10.03	-10.08	-11.00	-10.15	8.50	-10.05
HBY097	-8.18	-7.97	8.04	-6.69	-7.63	-7.43
ETR	-10.60	-10.21	-10.78	-9.60	-11.65	-11.58
RPV	-10.06	-9.11	-11.03	-11.18	-11.68	-12.62

The results of overlaying the native ligand and the re-docked ligand within the different crystal structures of HIV-1 RT complexed with various ligands are presented in Figure 2. Among the different crystal structures of HIV-1 RT complexed with various ligands, the three structures with the lowest RMSD values were 1FK9 (EFV), 3MEC (ETR), and 4G1Q (RPV), with corresponding values of 0.23 Å, 0.40 Å, and 0.51 Å, respectively. The RMSD threshold commonly used for accurate ligand binding pose reproduction is 2 Å which indicates that the ligand binding poses are considered to be accurately reproduced when the RMSD value is below this threshold.

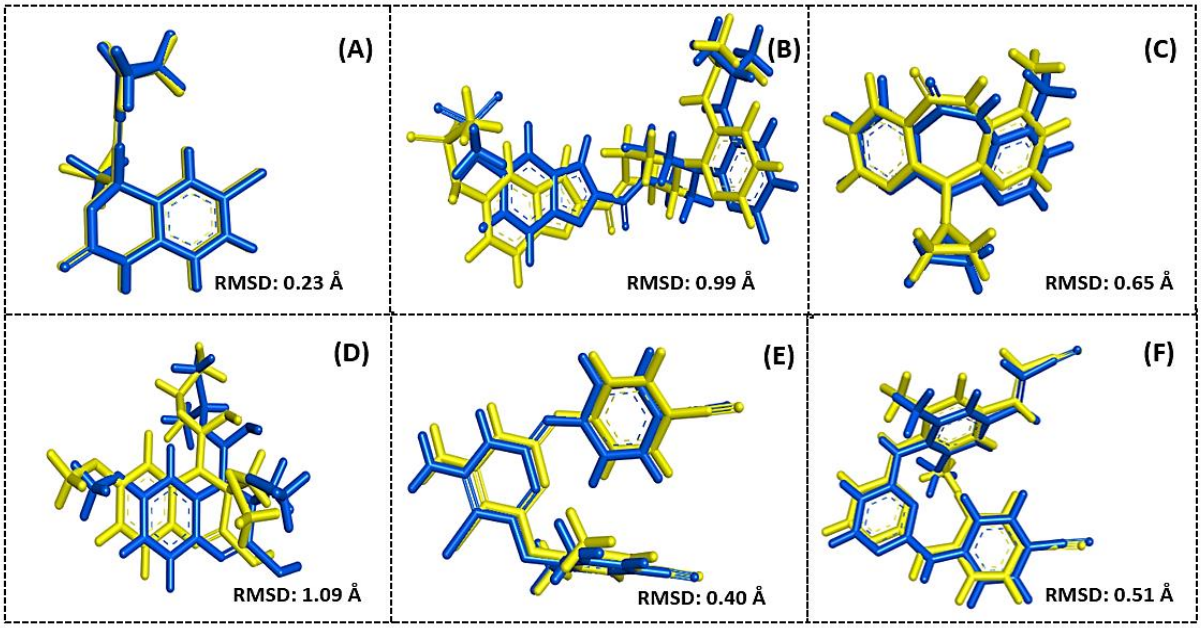

Figure 2 The validation of the docking method by overlaying the native ligand (blue) and the redocked ligand (yellow) within the binding pocket of HIV-1 RT crystal structures. (A) 1FK9 (EFV), (B) 1KLM (DLV), (C) 1VRT (NVP), (D) 2IC3 (HBY097), (E) 3MEC (ETR), and (F) 4G1Q (RPV).

In this study, the 4G1Q conformation of HIV-1 RT was chosen for further analysis and investigation. This decision was based on several factors. Firstly, it had a lower binding energy, indicating

a stronger binding affinity. The structure also showed a low RMSD value, indicating good alignment with the native ligand. Additionally, the 4G1Q structure had a relatively low resolution of 1.51 Å, as obtained from the RCSB PDB, indicating a high-quality crystal structure. The binding region of these ligands in HIV-1 RT corresponded with the NNRTI pocket, in which the active ligands against HIV-1 RT interacted with the amino acid residues within a 3.0 Å diameter centered at the ligands PRO95, LYS101, LYS103, VAL106, VAL179, TYR181, TYR183, TYR188, PRO225, PRO226, PHE227, TRP229, HIS235, PRO236, and TYR318 in the substrate binding pocket of HIV-1 RT via hydrogen bonding and hydrophobic interactions.

The molecular docking results are shown in Figure 3, indicating that all selected ligands were bound to the hydrophobic cavity in the binding pocket of HIV-1 RT (Figure 3A). Moreover, the overlaying of each selected ligand in the binding pocket revealed that all ligands bound in a similar region (Figure 3B). In addition, the crystal structure 4G1Q of the HIV-1 RT enzyme in a complex with RPV corresponded with the inhibitory activity against HIV-1 RT. A previous report also showed that RPV provided the most potential inhibition of nonnucleoside reverse transcriptase inhibitors (NNRTIs) [10, 32]. Consequently, 4G1Q was selected for further study as the most suitable crystal structure for the binding interaction between ligands and HIV-1 RT.

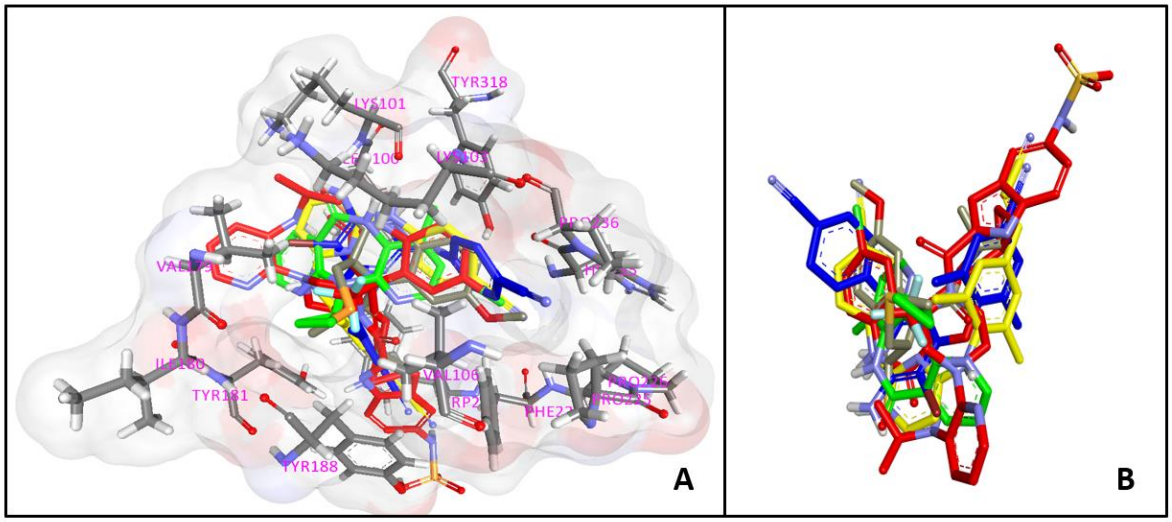

Figure 3 (A) The docking conformation of the analyzed ligands in HIV-1 RT (4G1Q) using molecular docking. (B) Overlaying of the conformations of NNRTI drugs EFV (pink), DLV (red), NVP (green), HBY097 (gray), ETR (blue) and RPV (yellow) in the binding pocket of HIV-1 RT.

Investigation of binding interaction between designed drug and HIV-1 RT

In this study, the binding interaction between amino-oxy-diarylquinoline derivatives, namely 4-(2′,6′-dimethyl-4′-cyanophenoxy)-6-(4″-cyanophenyl)-aminoquinoline **(1)** and 4-(2′,6′-dimethyl-4′-cyanophenoxy)-2-(4″-cyanophenyl)-aminoquinoline **(2)**, and NNRTIs drugs (NVP, EFV, HBY097, ETR, and RPV) were investigated, as shown in Figure 4 and Table 2. From the molecular docking results, it was found that the conventional hydrogen bonding interactions between HIV-1 RT and NNRTIs drugs

were demonstrated as between the N atom of the NH_2 group in LYS101 and the H atom of the NH group in those ligands. The hydrophobic interaction was performed using π-π stacking between TYR181, TYR188, TRP229 and TYR318 of HIV-1 RT and the benzene ring for ETR and RPV. In addition, compound **(1)** is also bound to LYS103 via H-bonding interactions between the H atom of the NH_2 group in LYS103 and the N atom of the CN group in the sidechain of **(1)** (Figure 4F). Additionally, **(2)** interacted with LYS101 via H-bonding interactions between the H atom of the NH_2 group in LYS101 and the N atom in the quinoline core structure of (2) (Figure 4G). Moreover, **(2)** formed LYS101 using H-bonding interactions between the O atom of the C=O amide group in LYS101 and the H atom of the NH group in the sidechain of **(2)**. Hydrophobic interactions were found in the TYR181, TYR188, and TRP229 residues of HIV-1 RT using π-π stacking interactions with aromatics in compounds **(1)** and **(2)**. The interaction of **(2)** in the binding pocket of HIV-1 RT was similar to that of NVP, EFV, and RPV because those ligands formed two conventional hydrogen bonds with LYS101.

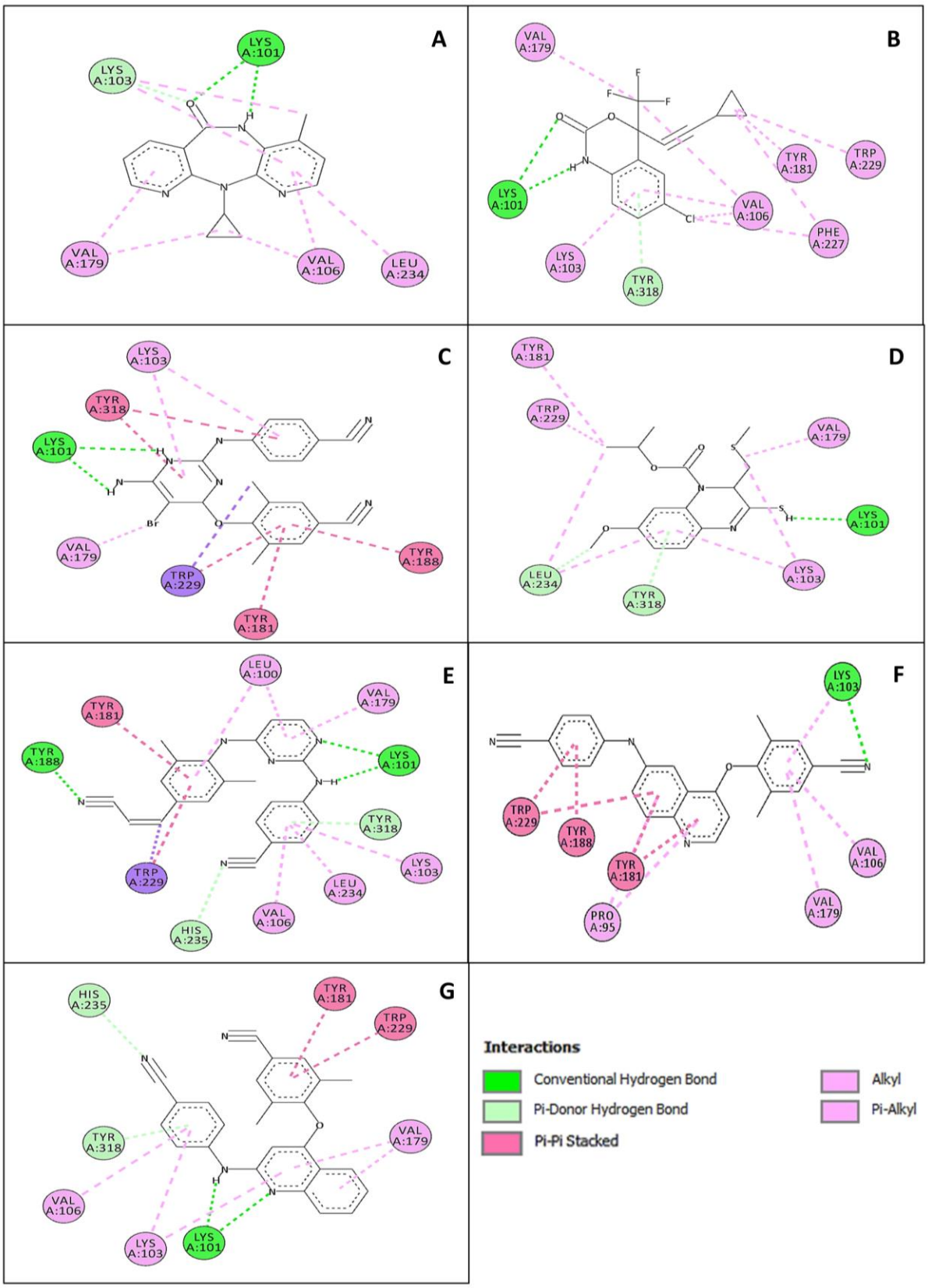

Figure 4 2D diagram showing the types of contacts formed between (NVP) (A), (EFV) (B), (ETR) (C), (HBY097) (D) (RPV) (E), **(1)** (F) and **(2)** (G) and HIV-1 RT.

Table 2 The results of molecular docking between ligands with HIV-1 RT (4G1Q.pdb).

Ligand	Binding Energy (kcal/mol)	Hydrogen bond	π-π Stacking
NVP	-8.39	LYS101	-
EFV	-9.25	LYS101	-
HBY097	-7.43	LYS101	-
ETR	-11.58	LYS101	TYR181 TYR188 TRP229 TYR318
RPV	-12.62	LYS101 TYR188	TYR181 TRP229
(1)	-12.07	LYS103	TYR181 TYR188 TRP229
(2)	-13.65	LYS101	TYR181 TRP229

Molecular Dynamic Simulations

Molecular dynamics (MD) simulations were employed to analyze the binding stability between ligands and the target protein in order to investigate the stability and conformational changes in a solvent environment. To assess the binding stability of RPV, **(1)** and **(2)** at the binding site of HIV-1 RT, several parameters, namely root mean square deviation (RMSD), root mean square fluctuation (RMSF), and radius of gyration (Rg), were examined over a 50 ns MD simulation. The RMSD served as an indicator of binding stability and the equilibrium state of the complex in the simulated system. The RMSF analysis provided insights into the fluctuation of amino acid residues during the MD simulation. Additionally, the Rg value was used to assess the compactness of the protein structure throughout the MD simulation process [33,34]. The RMSD calculations for HIV-1 RT and the HIV-1 RT complexes (RPV, **(1)**, and **(2)**) are shown in Figure 5A. The analysis reveals that the RMSD values of HIV-1 RT-**(1)** and HIV-1 RT-**(2)** are lower compared to HIV-1 RT-free and HIV-1 RT-RPV.

This suggests that HIV-1 RT-**(1)** and HIV-1 RT-**(2)** may have a more stable binding to HIV-1 RT. The lower RMSD values indicate that the conformations of HIV-1 RT-**(1)** and HIV-1 RT-**(2)** are relatively closer to the initial structure, implying a stronger interaction between the ligands and the protein. Figure 5B illustrates the RMSF calculations for HIV-1 RT and its complexes with RPV, **(1)**, and **(2)**. It can be observed that RMSF values of HIV-1 RT-RPV and HIV-1 RT-**(2)** at LYS101, TYR181, and TRP229 are lower compared to HIV-1 RT-free. This finding suggests that RPV and **(2)** establish interactions within the active site of HIV-1 RT, specifically involving the LYS101, TYR181, and TRP229 residues. In part of HIV-1 RT-**(1)**, the RMSF values at TYR181, TYR188, and TRP229 are lower than those of HIV-1 RT-free. This indicates that **(1)** also engages in interactions within the active site of HIV-1 RT, specifically involving the TYR181, TYR188, and TRP229 residues.

These observations are consistent with the binding interactions predicted by the molecular docking studies (as shown in Table 2). The lower RMSF values at specific residues in the HIV-1 RT-**(1)** and HIV-1 RT-**(2)** complexes suggest a more restrained and stable binding of the ligands to the HIV-1 RT. Furthermore, Figure 5C depicts the radius of gyration (Rg) for HIV-1 RT and its complexes

with RPV, **(1)**, and **(2)**. In the Rg graph, we can observe that the Rg values of the HIV-1 RT complexes (RPV, **(1)**, and **(2)**) are lower compared to the Rg value of HIV-1 RT-free. This indicates that the binding of RPV, **(1)**, and **(2)** to HIV-1 RT results in a more compact and stable protein structure. The lower Rg values suggest that the binding of these ligands promotes a more tightly packed conformation of the protein, potentially leading to enhanced stability of the complexes. This observation is consistent with the lower RMSD values, indicating that the conformations of HIV-1 RT-**(1)** and HIV-1 RT-**(2)** are more compact and stable during the binding interaction process.

Therefore, the results obtained from the MD simulation of these complexes suggest that the lower RMSD values, lower RMSF values at key residues, and lower Rg values observed for HIV-1 RT-**(1)** and HIV-1 RT-**(2)** compared to HIV-1 RT-free indicate a more stable and compact conformation of the protein in the presence of these ligands. These findings strongly support the potential of these ligands as promising candidates for further development as anti-HIV-1 agents.

Binding Free Energy Calculations

The Molecular Mechanics/Poisson-Boltzmann surface area (MMPBSA) and Molecular Mechanics/Generalized Born surface area (MMGBSA) methods are commonly employed to determine the binding free energies between proteins and designed drugs by considering various energy components, such as van der Waals interactions, electrostatic interactions, solvation energies, and entropy contributions [28,35]. The binding free energy between these ligands (RPV, **(1)**, and **(2)**) and HIV-1 RT was calculated using the MMPBSA and MMGBSA approaches [29]. The results obtained from the MMPBSA and MMGBSA calculations indicated that RPV, **(1)**, and **(2)** are bound to HIV-1 RT, as shown in Table 3.

The MMPBSA binding free energies of RPV, (1), and (2) bound to HIV-1 RT were determined as -55.08 ± 3.44, -45.74 ± 2.38, and -54.33 ± 2.57 kcal/mol, respectively. From Table-3, the MMGBSA binding free energies of RPV, (1), and (2) with HIV-1 RT were found to be -57.88 ± 3.44, -48.89 ± 2.41, and -56.94 ± 2.61 kcal/mol, respectively. Regarding the energy components, the Van der Waals interaction energies of HIV-1 RT-RPV, HIV-1 RT-**(1)**, and HIV-1 RT-**(2)** were observed to be -60.68 ± 3.09, -50.45 ± 2.28, and -57.29 ± 2.66 kcal/mol, respectively. RPV and **(2)** exhibited efficient binding energies with HIV-1 RT, demonstrating lower binding energy compared to **(1)**. These results indicate that the binding activity of **(2)** is similar to that of RPV. Furthermore, the calculated binding energies of these complexes demonstrated that the binding interaction of HIV-1 RT-**(2)** was more stable than HIV-1 RT-**(1)**, which is consistent with the binding energy obtained from the molecular docking studies (Table 2). Therefore, the results suggest that 4-(2′,6′-dimethyl-4′-cyanophenoxy)-2-(4″-cyanophenyl)-aminoquinoline **(2)** can be explored as a potential drug candidate for the development of new anti-HIV-1 RT agents.

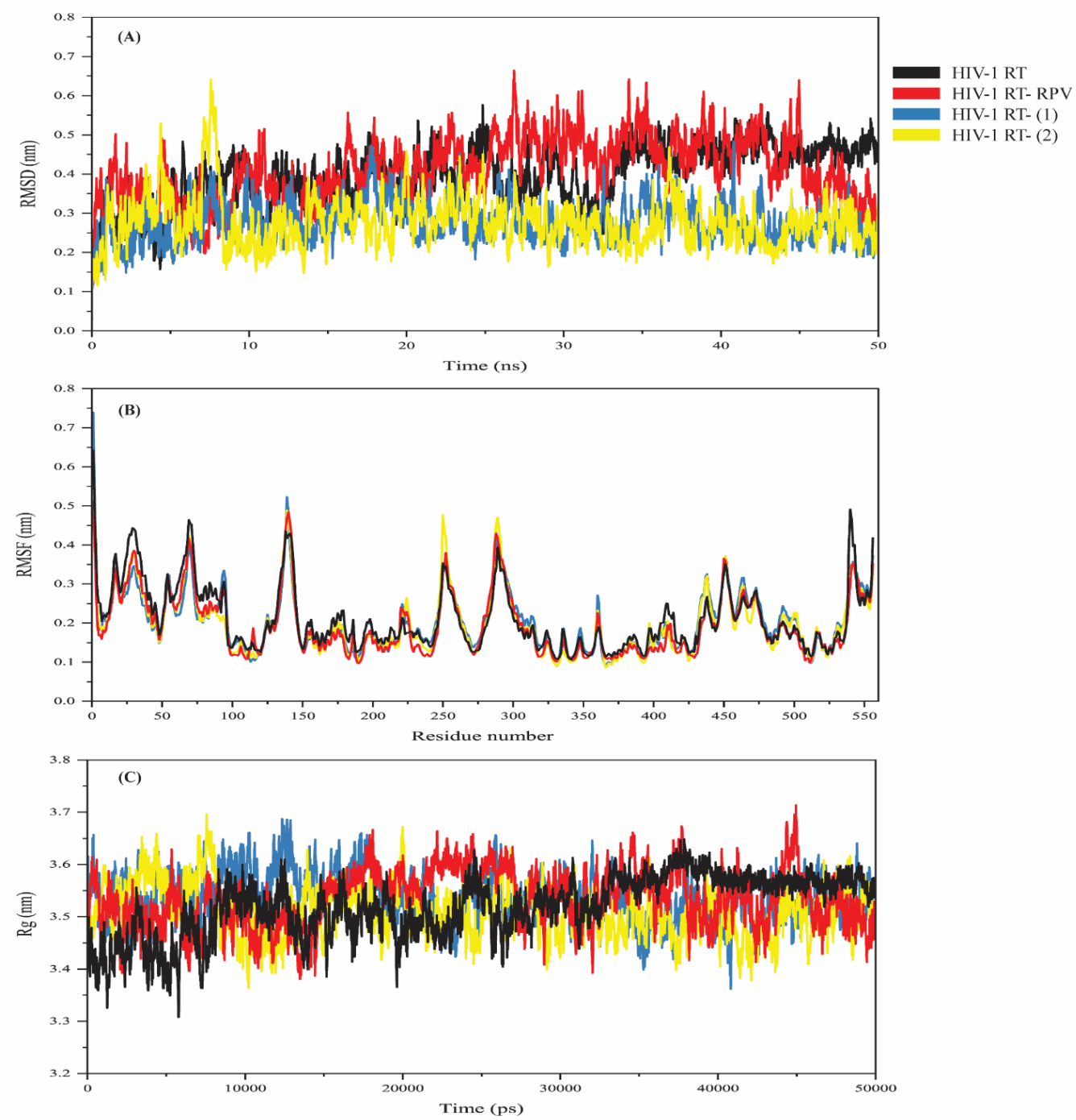

Figure 5 Superimposed structure of HIV-1 RT from MD simulation of HIV-1 RT, HIV-1 RT-RPV, HIV-1 RT-**(1)**, and HIV-1 RT-**(2)**. (A) RMSD graphs of HIV-1 RT, HIV-1 RT-RPV, HIV-1 RT-**(1)**, and HIV-1 RT-**(2)**. (B) RMSF graphs of HIV-1 RT, HIV-1 RT-RPV, HIV-1 RT-**(1)**, and HIV-1 RT-**(2)**. (C) Rg graphs of HIV-1 RT, HIV-1 RT-RPV, HIV-1 RT-**(1)**, and HIV-1 RT-**(2)**.

Table 3 Binding energies and individual component energy values obtained from the MMP-BSA and MMGBSA calculation of HIV-1 RT-RPV, HIV-1 RT-**(1)**, and HIV-1 RT-**(2)** complexes.

Energetic terms (kcal/mol)	HIV-1 RT-RPV	HIV-1 RT-**(1)**	HIV-1 RT-**(2)**
ΔE_{vdw}	-60.68 ± 3.09	-50.45 ± 2.28	-57.29 ± 2.66
ΔE_{ele}	-4.51 ± 0.80	-0.22 ± 0.85	-3.98 ± 0.68
ΔE_{MM}	-65.19 ± 2.98	-50.67 ± 2.41	-61.27 ± 2.55
ΔG_{IE}	6.56 ± 1.65	3.26 ± 0.76	4.29 ± 0.33
ΔG_{PB}	7.78 ± 0.60	5.14 ± 0.63	6.75 ± 0.41
$\Delta G_{non\text{-}polar/PB}$	-4.24 ± 0.10	-4.47 ± 0.09	-4.09 ± 0.11
$\Delta G_{solv/PB}$	3.54 ± 0.61	0.67 ± 0.65	2.66 ± 0.41
$\Delta G_{bind/PB}$	-55.08 ± 3.44	-45.74 ± 2.38	-54.33 ± 2.57
ΔG_{GB}	7.34 ± 0.59	4.71 ± 0.71	6.41 ± 0.42
$\Delta G_{nonpolar/GB}$	-6.59 ± 0.19	-6.19 ± 0.17	-6.36 ± 0.18
$\Delta G_{solv/GB}$	0.75 ± 0.60	-1.48 ± 0.71	0.04 ± 0.45
$\Delta G_{bind/GB}$	-57.88 ± 3.44	-48.89 ± 2.41	-56.94 ± 2.61

ΔE_{vdw}: Van der Waals energy; ΔE_{ele}: electrostatic energy; ΔE_{MM}: equal to the sum of the electro-static (ΔE_{ele}) and Van der Waals (ΔE_{vdw}) interactions; ΔG_{IE}: Interaction entropy; ΔG_{PB}: The Polar solvation free energy received from the Poisson Boltzmann method. $\Delta G_{non\text{-}polar/PB}$: Non-polar solvation energy from the Poisson Boltzmann method; $\Delta G_{solv/PB}$: Solvation energy from the Poisson Boltzmann method; $\Delta G_{bind/PB}$: Binding free energy received from the Poisson Boltzmann method. ΔG_{GB}: The Polar solvation free energy received from the generalised Born method. $\Delta G_{non\text{-}polar/GB}$: Non-polar solvation energy from the generalised Born method. $\Delta G_{solv/GB}$: Solvation energy from the generalised Born method; $\Delta G_{bind/GB}$: Binding free energy received from the generalised Born method

Conclusion

The goal of this study is to demonstrate the conformations of HIV-1 RT with NNRTIs and amino-oxy-diarylquinolines using cross-docking, molecular docking, and molecular dynamics simulations. Cross-docking investigation revealed that 4G1Q had a lower binding energy, RMSD value, and resolution when compared to the other conformations of HIV-1 RT. The binding free energy values between the ligands and HIV-1 RT ranged from -7.43 to -12.62 kcal/mol, with rilpivirine being the lowest at -12.62 kcal/mol. 4-(2′,6′-dimethyl-4′-cyanophenoxy)-6-(4′′-cyanophenyl)-aminoquinoline **(1)** and 4-(2′,6′-dimethyl-4′-cyanophenoxy)-6-(4′′-cyanophenyl)-aminoquinoline **(2)** were designed to develop a binding interaction and inhibit HIV-1 RT. Molecular docking revealed that **(2)**, similar rilpivirine, interacts with LYS101 residues via two hydrogen bonds and with TYR188 and TRP229 residues via π-π stacking in HIV-1 RT. Furthermore, the molecular dynamics simulations conducted in

this study demonstrated the stability of the binding between **(1)** and **(2)** with HIV-1 RT. The MMPBSA and MMGBSA calculations indicated that HIV-1 RT-**(2)** had a lower binding free energy than HIV-1 RT-**(1)**. As a result, the conformation of 4G1Q is thought to be the most suited for the binding interaction between ligands and HIV-1 RT, and the 2-amino-4-phenoxy-substituted quinoline molecule offers significant promise as a fundamental platform for the development of anti-HIV-1 agents.

Acknowledgements

The authors are grateful to the Chulabhorn Research Institute and Thailand Science Research and Innovation (TSRI) for financial support (Grant No. 36826) during this study.

References

1. Gu S-X, Zhu Y-Y, Wang C, Wang H-F, Liu G-Y, Cao S, et al. Recent discoveries in HIV-1 reverse transcriptase inhibitors. Curr Opin Pharmacol. 2020;54:166-72.
2. Xiao T, Tang J-F, Meng G, Pannecouque C, Zhu Y-Y, Liu G-Y, et al. Indazolyl-substituted piperidin-4-yl-aminopyrimidines as HIV-1 NNRTIs: Design, synthesis and biological activities. Eur J Med Chem. 2020;186:111864.
3. Popović-Djordjević J, Quispe C, Giordo R, Kostić A, Stanković JSK, Fokou PVT, et al. Natural products and synthetic analogues against HIV: A perspective to develop new potential anti-HIV drugs. Eur J Med Chem. 2022;233:114217.
4. Wang Z, Cherukupalli S, Xie M, Wang W,Jiang X, Jia R, et al. Contemporary medicinal chemistry strategies for the discovery and development of novel HIV-1 non-nucleoside reverse transcriptase inhibitors. J Med Chem. 2022;65(5):3729-57.
5. Steegen K, Bronze M, Papathanasopoulos MA, van Zyl G, Goedhals D, Variava E, et al. HIV-1 antiretroviral drug resistance patterns in patients failing NNRTI-based treatment: results from a national survey in South Africa. J Antimicrob Chemother. 2017;72(1):210-9.
6. Bossard C, Schramm B, Wanjala S, Jain L, Mucinya G, Opollo V, et al. High prevalence of NRTI and NNRTI drug resistance among ART-experienced, hospitalized inpatients. J Acquir Immune Defic Syndr. 2021;87(3):883-8.
7. Kang D, Ruiz FX, Sun Y, Feng D, Jing L, Wang Z, et al. 2,4,5-Trisubstituted pyrimidines as potent HIV-1 NNRTIs: rational design, synthesis, activity evaluation, and crystallographic studies. J Med Chem. 2021;64(7):4239-56.
8. Rebeiro PF, Jenkins CA, Bian A, Lake JE, Bourgi K, Moore RD, et al. Risk of incident diabetes mellitus, weight gain, and their relationships with integrase inhibitor–based initial antiretroviral therapy among persons with human immunodeficiency virus in the United States and Canada. Clin Infect Dis. 2021;73(7):E2234-42.
9. Crowell TA, Danboise B, Parikh A, Esber A, Dear N, Coakley P, et al. Pretreatment and acquired antiretroviral drug resistance among persons living with HIV in four African countries. Clin Infect Dis. 2021;73(7):E2311-22.

10. Makarasen A, Kuno M, Patnin S, Reukngam N, Khlaychan P, Deeyohe S, et al. Molecular docking studies and synthesis of amino-oxydiarylquinoline derivatives as potent non-nucleoside HIV-1 reverse transcriptase inhibitors. Drug Res. 2019;69(12):671-82.
11. Techasakul S, Makarasen A, Reuk-ngam N, Khlaychan P, Kuno M, Hannongbua S. Derivatives and composition of quinoline and naphthyridine. WO Patent 2019045655A1, filed 29 August 2017, and issued 7 March 2019.
12. Ragno R, Frasca S, Manetti F, Brizzi A, Massa S. HIV-reverse transcriptase inhibition: inclusion of ligand-induced fit by cross-docking studies. J Med Chem. 2005;48(1):200-12.
13. Lannutti F, Marrone A, Re N. Binding of GSH conjugates to -GST: A cross-docking approach. J Mol Graph. 2012;32:9-18.
14. Wang Y, Wang A, Wang J, Wu X, Sun Y, Wu Y. Me-Better Drug design based on nevirapine and mechanism of molecular interactions with Y188C mutant HIV-1 reverse transcriptase. Molecules. 2022;27(21):7348.
15. Singh K, Marchand B, Rai DK, Sharma B, Michailidis E, Ryan EM, et al. Biochemical Mechanism of HIV-1 resistance to rilpivirine. J Biol Chem. 2012;287(45):38110-23.
16. Aeksiri N, Songtawee N, Gleeson MP, Hannongbua S, Choowongkomon K. Insight into HIV-1 reverse transcriptase–aptamer interaction from molecular dynamics simulations. J Mol Model. 2014;20(8):2380.
17. Morris GM, Huey R, Lindstrom W, Sanner MF, Belew RK, Goodsell DS, et al. AutoDock4 and AutoDock-Tools4: automated docking with selective receptor flexibility. J Comput Chem. 2009;30(16):2785-91.
18. Frisch MJ, Trucks GW, Schlegel HB, Scuseria GE, Robb MA, Cheeseman JR, et al. Gaussian 09, Revision, B.01; Gaussian Inc.: Wallingford, CT, USA, 2010.
19. Ren J, Milton J, Weaver K L, Short SA, Stuart DI, Stammers DK. Structural basis for the resilience of efavirenz (DMP-266) to drug resistance mutations in HIV-1 reverse transcriptase. Structure. 2000;8(10):1089-94.
20. Esnouf RM, Ren J, Hopkins AL, Ross CK, Jones EY, Stammers DK, et al. Unique features in the structure of the complex between HIV-1 reverse transcriptase and the bis(heteroaryl)piperazine (BHAP) U-90152 explain resistance mutations for this nonnucleoside inhibitor. Proc Natl Acad Sci U S A. 1997;94(8):3984–9.
21. Ren J, Esnouf R, Garman E, Somers D, Ross C, Kirby I, et al. High resolution structures of HIV-1 RT from four RT-inhibitor complexes. Nat Struct Biol. 1995;2(4):293-302.
22. Das K, Sarafianos SG, Clark Jr AD, Boyer PL, Hughes SH, Arnold E. Crystal structures of clinically relevant Lys103Asn/Tyr181Cys double mutant HIV-1 reverse transcriptase in complexes with ATP and non-nucleoside inhibitor HBY 097. J Mol Biol. 2007;365(1):77-89.
23. Lansdon EB, Brendza KM, Hung M, Wang R, Mukund S, Jin D, et al. Crystal structures of HIV-1 reverse transcriptase with etravirine (TMC125) and rilpivirine (TMC278): implications for drug design. J Med Chem. 2010;53(10):4295-99.

24. Kuroda DG, Bauman JD, Challa JR, Patel D, Troxler T, Das K, et al. Snapshot of the equilibrium dynamics of a drug bound to HIV-1 reverse transcriptase. Nat Chem. 2013;5(3):174-81.
25. Hornak V, Abel R, Okur A, Strockbine B, Roitberg A, Simmerling C. Comparison of multiple Amber force fields and development of improved protein backbone parameters. Proteins. 2006;65(3):712-25.
26. Humphrey W, Dalke A, Schulten K. VMD: visual molecular dynamics. J Mol Graph. 1996;14(1):33-8.
27. Altharawi A. Targeting Toxoplasma gondii ME49 TgAPN2: a bioinformatics approach for antiparasitic drug discovery. Molecules. 2023;28(7):3186.
28. Virtanen SI, Niinivehmas SP, Pentikäinen OT. Case-specific performance of MM-PBSA, MM-GBSA, and SIE in virtual screening. J Mol Graph Model. 2015;62:303-18.
29. Valdés-Tresanco MS, Valdés-Tresanco ME, Valiente PA, Moreno E. gmx_MMPBSA: a New tool to perform end-state free energy calculations with GROMACS. J Chem Theory Comput. 2021;17(10):6281-91.
30. Zubair MS, Maulana S, Widodo A, Mukaddas A, Pitopang R. Docking study on anti-HIV-1 activity of secondary metabolites from Zingiberaceae plants. J Pharm Bioallied Sci. 2020;12(2):763-7.
31. Kumar A, Zhang KYJ. A cross docking pipeline for improving pose prediction and virtual screening performance. J Comput Aided Mol Des. 2018;32(1):163-73.
32. Makarasen A, Patnin S, Vijitphan P, Reukngam N, Khlaychan P, Kuno M, et al. Structural basis of 2-phenylamino-4-phenoxyquinoline derivatives as potent HIV-1 non-nucleoside reverse transcriptase inhibitors. Molecules. 2022;27(2):461-81.
33. Wan Y, Tian Y, Wang W, Gu S, Jua X, Liu G. In silico studies of diarylpyridine derivatives as novel HIV-1 NNRTIs using docking-based 3D-QSAR, molecular dynamics, and pharmacophore modeling approaches. RSC Adv. 2018;8(71):40529-43.
34. Sathiyamani B, Daniel EA, Ansar S, Esakialraj BH, Hassan S, Revanasiddappa PD, et al. Structural analysis and molecular dynamics simulation studies of HIV-1 antisense protein predict its potential role in HIV replication and pathogenesis. Front Microbiol. 2023;14:1152206.
35. Korlepara DB, Vasavi CS, Jeurkar S, Pal PK, Roy S, Mehta S, et al. PLAS-5k: dataset of protein-ligand affinities from molecular dynamics for machine learning applications. Sci Data. 2022;9(1):548.